Chapter 4

Experimental measure of dynamic heterogeneities and correlations near the glass transition temperature

4.1 Introduction

The glassy state of matter is an amorphous state which is achieved by rapidly cooling the material from its liquid or molten state through its glass transition temperature (T_g). In this state, the materials are rigid like solids but they lack the long-range structural order. During the process of glass formation, many interesting features start emerging like rapid slowdown of dynamics or increase in viscosity, growing amorphous order, physical aging and dynamic heterogeneities [1, 2, 3]. Despite years of research, the overall understanding of these dynamical features of the glassy state remains elusive. A popular approach towards the understanding of glass transition and the slow dynamics was established based on an intuitive picture that the molecules or atoms in the glass former are cooperatively rearranging with the decrease in temperature on going deeper into the glassy state. The existence of these cooperatively rearranging regions (CRRs) was first proposed by Adam and Gibbs in 1965 [4]. The understanding of glassy dynamics was further extended by random first-order theory (RFOT) which suggested the presence of cooperatively rearranging metastable states. The dynamic correlation length of these CRRs grows on going deeper into the glassy state [5]. Interestingly, many numerical simulations and experiments on glass-forming liquids and colloidal glasses provide evidence of a growing amorphous order in agreement with the RFOT

but the experimental validation for molecular liquids remains uncertain [6, 7].

The glassy dynamics is also known to be heterogeneous with fast and slow relaxing modes present in the glassy state which has been experimentally observed in colloidal glasses [7, 8, 9, 10]. Dynamic heterogeneity can therefore be defined as the spatiotemporal fluctuations in the glass-forming systems. Dynamic heterogeneity has so far been observed in a wide variety of systems like colloidal glasses, molecular glass-forming liquids, gels and granular media [6, 11, 12, 13]. More recently there has been evidence of the presence of dynamic heterogeneities in biological systems like, cells and tissues [14] where their collectively rearranging movements are correlated to the neighborhood during biological processes like organ regeneration and wound healing [6]. The dynamic heterogeneities can be quantified in the form of dynamic susceptibility (χ_4) [1, 15] which is an important parameter that can correctly predict the overall shape of the correlation function with a peak pointing towards the α relaxation time scale. The evolution of peak height in χ_4 gives the dynamic length scale (ξ_4) [15]. Dynamic susceptibility has been measured in various glass formers from colloids to polymeric glasses using simulations where the dynamic length scales and time scales are predicted [16, 17, 18, 19]. Several experiments have also been performed to quantify dynamic susceptibility and determine the growing correlation in colloids as well as molecular glass formers [7, 20, 21]. Both simulations and experimental results suggest that the structural relaxation dynamics and the growing correlations in a glass follow a non-exponential character [19, 21]. Recent simulations on glassy polymers have shown a clear distinction between the fast and slow relaxing process (α and β relaxations) in four-point correlation functions [22]. Simulations have also predicted that the glassy dynamics have a structural correlation that increases with decreasing temperature [18]. Although effort has been made to study the microscopic origin and structural correlation of glassy dynamics but a clear understanding and direct experimental evidence is still lacking. In the present study, we aim to provide direct experimental evidence of the presence of dynamic heterogeneities in a polymer glass at a molecular scale using Raman spectroscopy.

Raman spectroscopy being vibrational spectroscopy provide information about molecular vibrations and their variation as a function of external perturbation. The α, β, and γ relaxation dynamics have been studied using Raman spectroscopy for Nylon 6,6 [23]. Therefore, Raman spectroscopy is

suitable to provide insights into the molecular dynamics, and the fast and slow relaxation processes occurring during the formation of a glass. A study of the correlations of a suitable fluctuating quantity such as polarization (Raman scattered intensity) fluctuations can also yield very useful information both on the dynamics as well as thermodynamics of the glassy state [24, 25]. This motivates us to explore the glassy dynamics with the help of Raman spectroscopy. In this chapter, we have explored the cooperative nature of glassy dynamics and studied the presence of dynamic heterogeneities in a polymer glass using Raman spectroscopy. We have also attempted to determine the spatial and temporal correlations from the relaxing Raman modes. Finally, we have extracted the dynamic susceptibility from the Raman peak intensity and have observed the variation of dynamic susceptibility as a function of temperature and as a function of time after quenching.

4.2 Effect of thermal perturbations on unprocessed PVAc and PVAc film

The Raman spectrum of unprocessed PVAc has sharp peaks representing the different vibrational modes present in PVAc which were discussed in detail in Chapter 3. The thermal perturbations were applied to pass through the glass transition temperature (T_g), to drive the system in the glassy state as discussed in Chapter 3. The Raman spectrum of unprocessed PVAc is shown in Figure 4.1(a). The effect of the thermal ramp on the unprocessed PVAc is shown in Figure 4.1(b) which shows the behavior of I_{INT} during the thermal ramp in C-H stretching mode of unprocessed PVAc. The drastic change in I_{INT} with a temperature change indicates the presence of thermally activated relaxation processes induced into the polymer. Also, the effect of thermal quench is shown in Figure 4.1(c) where the fluctuations in I_{INT} represent the presence of thermally activated molecular mobility in unprocessed PVAc.

The effect of thermal perturbations is also studied in PVAc film, and the results are discrete. In PVAc film, the Raman spectrum shows enormous broadening as shown in Figure 4.2(a) which is mainly due to disorders present in the PVAc film and represented the amorphous nature of PVAc film as compared to unprocessed PVAc. Due to the presence of disorders, the Raman spectrum has two broad

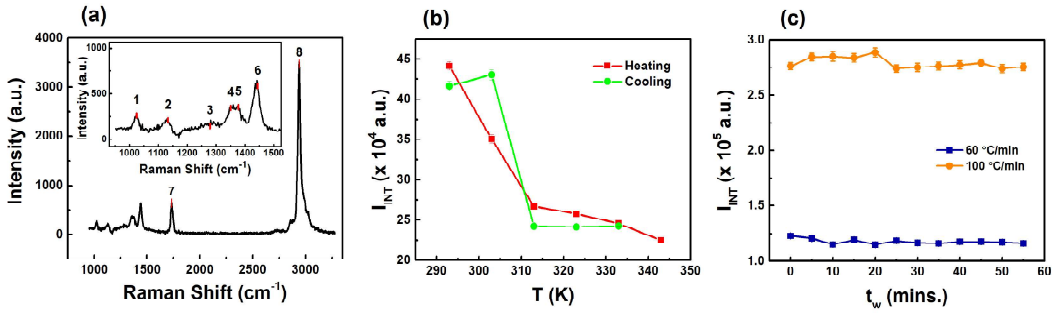

FIGURE 4.1: (a) Raman spectrum of unprocessed PVAc and its representative vibrational modes numbered in red. The inset shows closely appearing modes in the Raman spectrum. (b) Variation in integrated intensity (I_{INT}) as a function of temperature during thermal ramp for heating and cooling cycles of peak 8 representing the C-H stretching vibrational modes. (c) Variation in integrated intensity (I_{INT}) as a function of waiting time after quench through the glass transition temperature (T_g) of peak 8 representing the C-H stretching vibrational modes.

bands which can be deconvoluted into three peaks as labeled in Figure 4.2(a). On subjecting PVAc film to a thermal ramp, a distinct variation in the configurational states is observed during the heating and cooling cycles of the PVAc film which is evident from the variation in I_{INT} as shown in Figure 4.2(b). On subjecting to thermal quench at two different quench rates a distinct evolution in the I_{INT} is observed for the C-H stretching mode in PVAc film. This evolution is a signature of thermally induced molecular mobility in the system.

From Figures 4.1 and 4.2 it is evident that the thermal perturbations are driving the polymer in its glassy state which is reflected in the form of induced molecular mobility and variable configurational states.

4.3 Correlations in Raman modes

The presence of intra-molecular mobility and the signature of thermally induced relaxations present in both the unprocessed PVAc and in PVAc film has been discussed in Chapter 3 which helped in determining the glassy dynamics of PVAc on exposing the polymer to the thermal perturbations (thermal ramp and thermal quench). To further extend the study, inter and intra-mode correlations

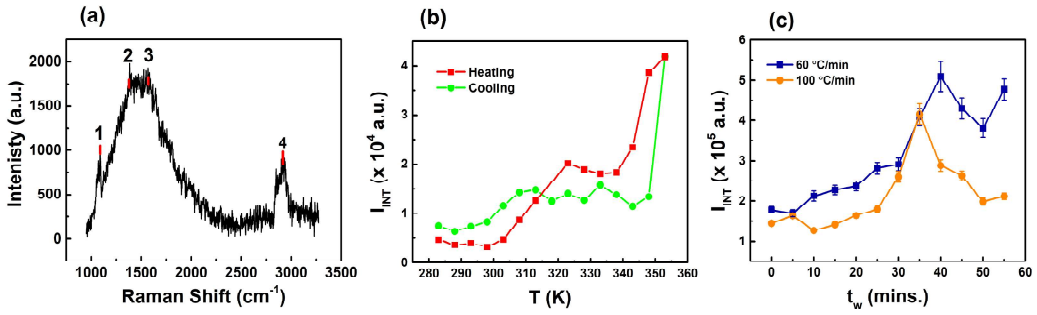

FIGURE 4.2: (a) Raman spectrum of PVAc film and its representative vibrational modes numbered in red. (b) Variation in integrated intensity (I_{INT}) as a function of temperature during thermal ramp for heating and cooling cycles of peak 4 representing the C-H stretching vibrational modes. (c) Variation in integrated intensity (I_{INT}) as a function of waiting time after quench through the glass transition temperature (T_g) at two different rates (60 °C/min and 100 °C/min) of peak 4 representing the C-H stretching vibrational modes.

are calculated between the Raman modes in unprocessed PVAc as well as in PVAc film.

Figure 4.3 represents the correlation matrix of Pearson's correlation coefficients calculated for all the temperatures during the heating and cooling cycle of the thermal ramp. A strong correlation is observed for both unprocessed PVAc and PVAc film during the thermal ramp with a Pearson's correlation coefficient higher than 0.55. In unprocessed PVAc, as shown in Figure 4.3 (a), the Raman modes are strongly correlated irrespective of their presence in the main chain or side branch of the polymer. Even the weaker peaks in the Raman spectrum like the C-H bending (peak 3) and CH_2 symmetric deformation (peak 4) are also positively correlated with other strong modes like C-C stretching (peak 1) and C-H stretching (peak 8) with a Pearson's correlation coefficient higher than 0.55. The strong correlation in the Raman modes hereby suggests that the polymer chain possesses strongly correlated dynamics which has also been observed as an effect of thermal quench in the segmental dynamics in Chapter 3 Figure 3.22(a) in unprocessed PVAc. In PVAc film, as shown in Figure 4.3(b), the there important peaks appearing in the Raman spectrum are found to be strongly correlated with a Pearson's correlation coefficient higher than 0.75

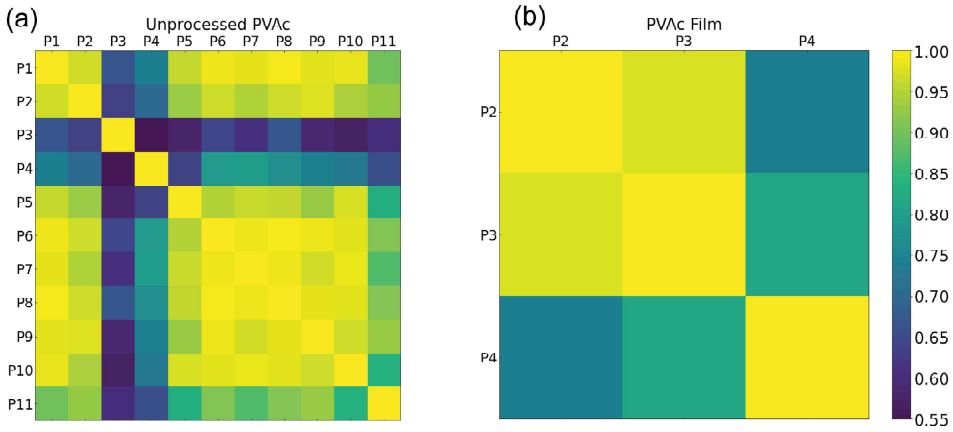

FIGURE 4.3: Correlation matrix of Pearson's correlation coefficients for all Raman modes present in the Raman spectrum of (a) unprocessed PVAc and (b) PVAc film during the heating and cooling cycles of the thermal ramp.

for all the peaks. This represents that the dynamics in PVAc film are also cooperative similar to the unprocessed PVAc. The correlation matrix, therefore, gives a signature of the cooperative polymer dynamics after the polymer is exposed to a thermal ramp.

During the thermal quench, the correlation matrix of Pearson's correlation coefficients shows a response different from the correlation matrix of the thermal ramp which is shown in Figure 4.4. For thermal quench, Pearson's correlation coefficients are calculated for the waiting time (t_w) after quenching through T_g at a rate of 60 °C/min. In unprocessed PVAc, unlike the thermal ramp, the temporal evolution in thermal quench shows a behavior varying from strongly correlated to strongly anti-correlated for different Raman modes. The stronger Raman modes present in the main chain and side branch of the polymer are found to be strongly correlated with a correlation coefficient higher than 0.5. The skeletal C–C stretching is strongly correlated to the CH_2 symmetric deformation, CH_2 scissoring, C-H symmetric and asymmetric stretching in CH_3 mode as evident from the correlation matrix shown in Figure 4.4 (a). The C-H stretching mode is also strongly correlated with the C-C stretching, C=O stretching, and CH_2 scissoring mode. However, the weaker modes, like C-H bending and CH_2 and CH_3 deformation show anti-correlation which can possibly be due to the difference in dynamics of different Raman modes after the thermal quench. In

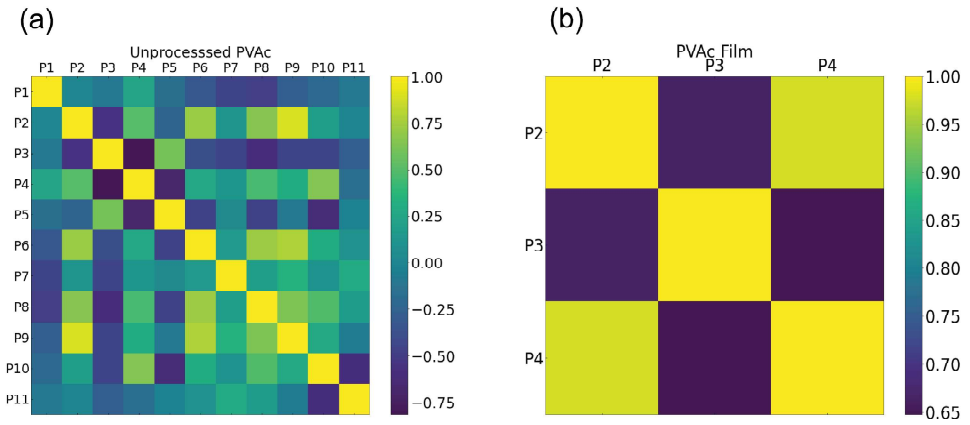

FIGURE 4.4: Correlation matrix of Pearson's correlation coefficients for all Raman modes present in the Raman spectrum of (a) unprocessed PVAc and (b) PVAc film for the time evolution of the Raman modes after quenching with a rate of 60 °C/min.

PVAc film, the Raman modes show a strong correlation with a Pearson's correlation coefficient higher than 0.65 as shown in Figure 4.4 (b). This suggests that the temporal evolution of the PVAc film is highly correlated.

For both thermal perturbations, thermal ramp, and thermal quench, the Raman modes of the polymer mostly show strong correlations for both the unprocessed and film state of the polymer. This indicates that the variations due to thermal perturbations in the main chain and the side branches of the polymer are cooperative. Since the Raman modes are indicators of molecular scale mobility in the polymer, therefore, it can be established that the thermal relaxation of PVAc in both bulk and film state are cooperative in nature. The cooperative nature of relaxation dynamics in PVAc and other molecular glasses has previously been observed using dielectric spectroscopy where the evolution of cooperatively rearranging regions was observed with time in the glassy state [20]. The presence of dynamic heterogeneities was also observed in the form of increasing correlations between the dynamically rearranging segments with increasing relaxation time [20].

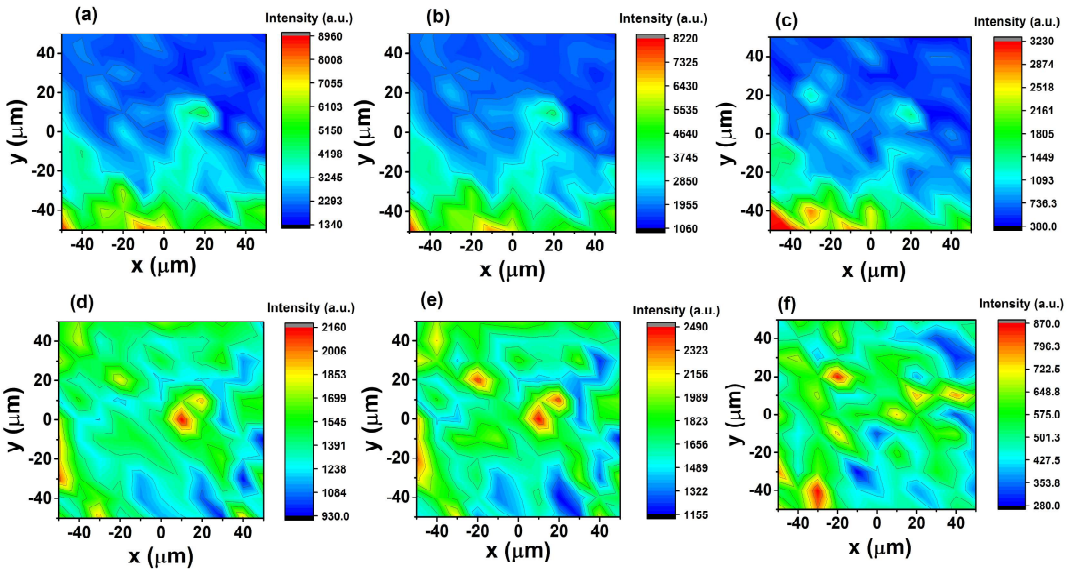

FIGURE 4.5: Spatial variation of peak intensities (I_{Max}) on a surface of 100 μm x 100 μm area on PVAc film for peaks 2, 3 and 4 appearing in the Raman spectrum (as labeled in Figure 4.2) (a) at room temperature and (b) after quenching at the rate of 60 °C/min.

4.4 Dynamic heterogeneities in glassy polymer

From the presence of correlation in the Raman peak intensity (I_{Max}) of PVAc film, it is evident that for both the perturbations, thermal ramp, and thermal quench, the molecular scale mobility in the polymer has a correlated motion. The dynamics of polymer is therefore cooperative which encourages to study of the presence of dynamically heterogeneous CRRs within the polymer matrix in its glassy state. For this purpose, a spatiotemporal mapping of PVAc film is performed using a Raman spectrometer for an area of 100 x 100 μm. The region is divided into 11 x 11 matrix points and a Raman spectrum is collected at each point along the space. The spectrum was collected in 1 minute with two acquisitions of 30 seconds each. The incident light focusses on each new point along the space with the help of a piezo probe controlled by the software.

2D maps of PVAc film over a region of 100 μm x 100 μm represent clusters of variable Raman peak intensity at variable space for all the three predominant modes in the Raman spectrum of PVAc film. When a glassy polymer undergoes thermal perturbation passing through T_g, it usually experiences a phenomenon

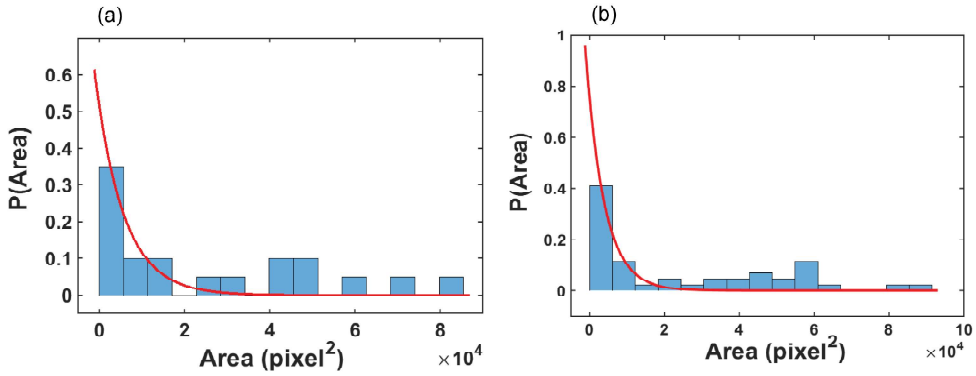

FIGURE 4.6: Domain size distribution of the heterogeneous domains in peak 4 representing C-H stretching mode of PVAc film across a region of 100x100 μm (a) before quench (at room temperature) and (b) after the quench (t_w = 0). The normalized distribution of area follows an exponential character which is represented by the exponential fit (red line).

known as aging where the polymer glass evolves through different free energy minima corresponding to different structural states. To study this phenomenon in 2 dimensions, the 2D maps were captured before and after quenching the polymer through T_g at a rate of 60 °C/min. Figure 4.5 (a), (b) and (c) represent the 2D maps of peaks 2, 3, and 4 respectively of PVAc film before quench (at room temperature) and Figure 4.5 (d), (e) and (f) represents the 2D maps of peaks 2, 3 and 4 respectively of PVAc film after the quench (t_w = 0). From the spatial variation of the peak intensities, it is evident that there is an enhancement in the number of clusters after quenching for all the peaks which can be seen from Figure 4.6 which shows the domain size distribution of heterogeneous domains in peak 4 of PVAc film. Before quenching, 20 domains of variable size are obtained with a mean area of 2.499 x 10^4 pixel^2 (1 pixel = 0.054 μm), and after quenching, the number increases to 44 domains with a mean area of 2.414 x 10^4 pixel^2 for peak 4 of PVAc film. The increase in the number of domains reflects the increase in heterogeneities in PVAc film which indicates that quenching has introduced CRRs in the polymer film, exhibiting time-evolution after quenching through T_g.

The mosaic of CRRs as seen in the 100 μm x 100 μm 2D map indicates the presence of dynamic heterogeneities in the polymer film. To analyze the time

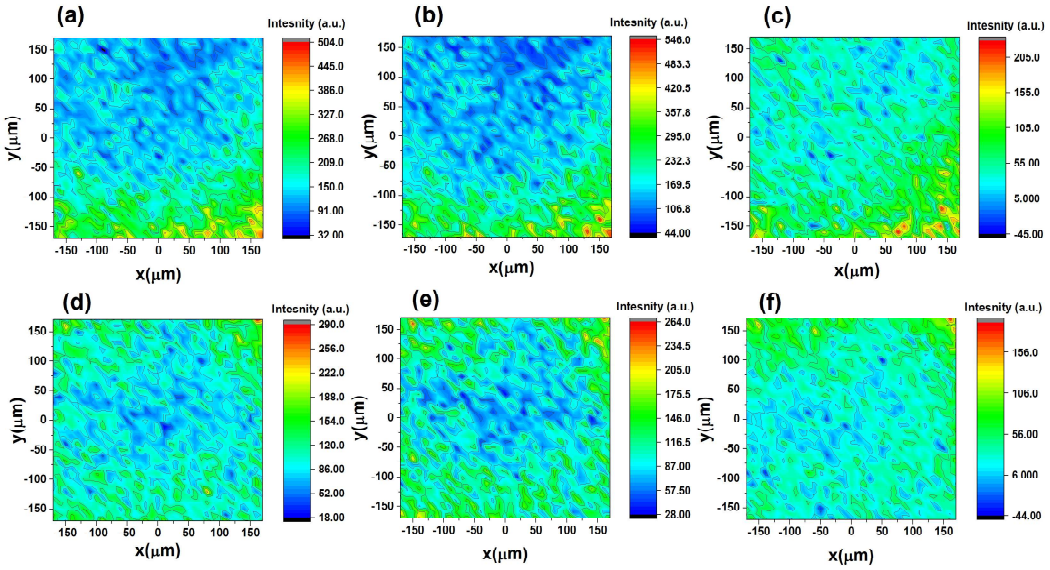

FIGURE 4.7: Time resolved spatial variation of peak intensities (I_{Max}) on a surface of 340 μm x 340 μm area on PVAc film for peaks 2, 3 and 4 appearing in the Raman spectrum (as labeled in Figure 4.2 (a) immediately after quenching (t_w = 0) at the rate of 60 °C/min and (b) 95 minutes after quenching (t_w = 95 min.).

evolution and the spatial extent of the dynamic heterogeneities, a time-resolved mapping is also performed for a larger space and faster time where an area of 340 x 340 μm is chosen which is divided into 35 x 35 matrix points at a distance of 10 μm each and Raman spectrum is collected at each point in 4 secs. by taking 2 acquisitions of 2 seconds each. The 2D map is collected instantly after quenching (t_w = 0) and after 95 minutes of quenching (t_w = 95 min.). Figure 4.7 (a), (b), and (c) represents the 2D map of peaks 2, 3, and 4 respectively of PVAc film at t_w = 0 and Figure 4.7 (d), (e) and (f) represents the 2D map of peaks 2, 3 and 4 respectively of PVAc film at t_w = 95 min. It is evident from the figure that the number of clusters increases as a function of time after quenching. It is also seen from the 2D cluster map that there are regions of variable intensity around the entire region of 340 μm x 340 μm which reveals spatial variability in the intensity of vibrational modes in different regions of the films. This variability changes after 95 minutes, indicating the presence of slow dynamics of possible CRRs in the system.

It is also interesting to see that the dynamic heterogeneities observed from the 2D Raman map has a fractal character. The boundaries of the heterogeneous clusters in 2D Raman maps are observed here to have fractal dimension. The

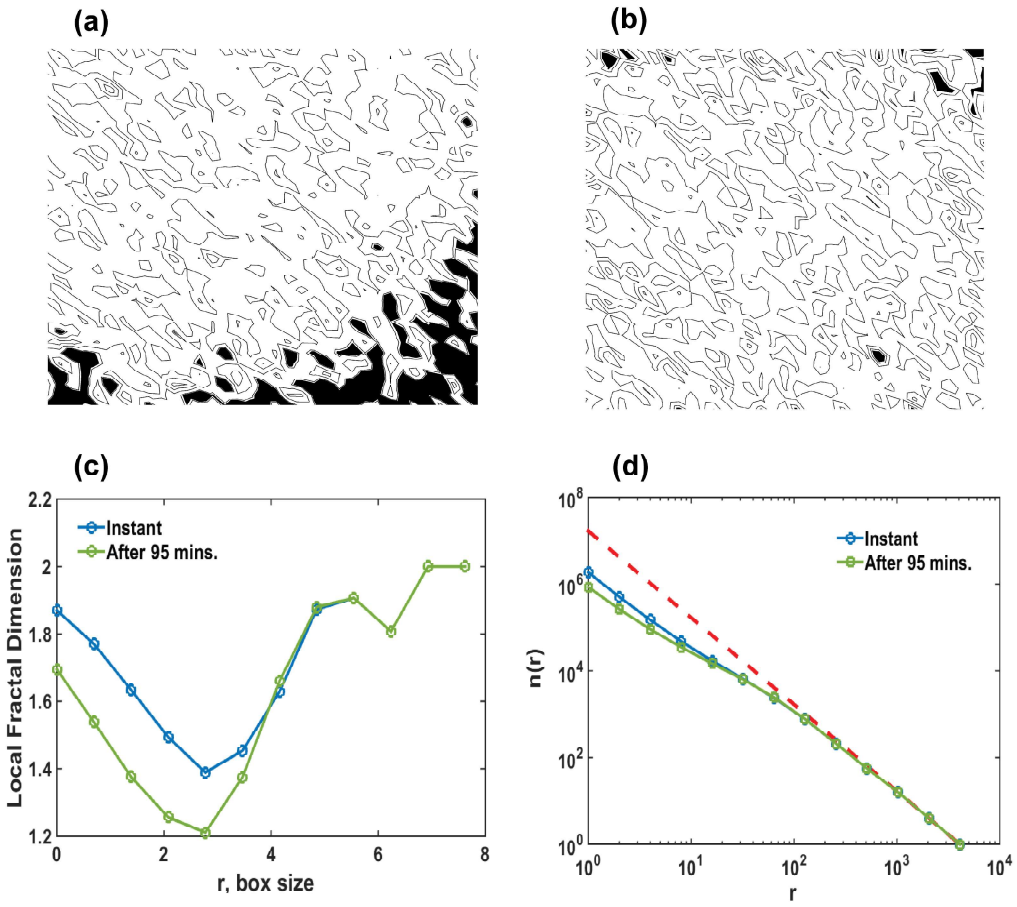

FIGURE 4.8: Binary plot of the heterogeneities in the two-dimensional contour plot of Raman intensity for P2 in PVAc film (a) at t_w = 0 and (b) at t_w = 95 min. The black borders were detected by the boxcount algorithm to calculate the fractal dimensions. (c) variation of local fractal dimension d_F as a function of box size (r) (d) the number of boxes (n(r)) versus r, box size and their power law fitting ($n(r) = r^{-d_F}$; dashed red line) which determines the fractal dimension of the polymer.

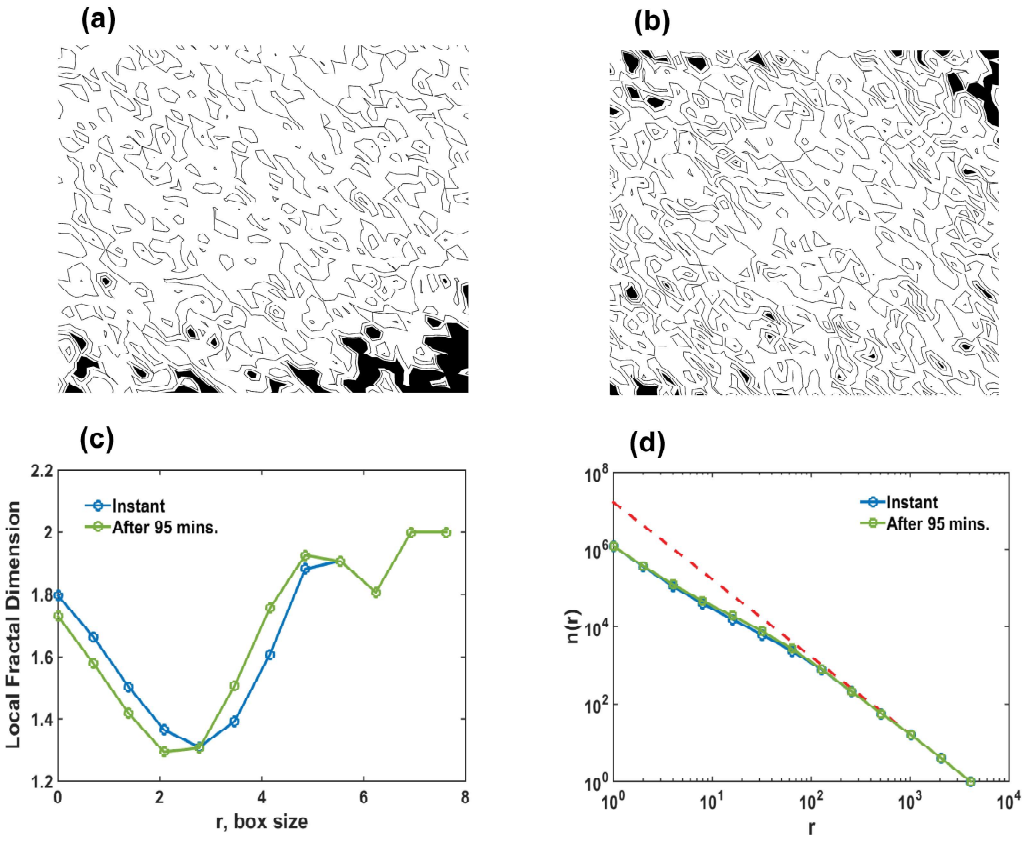

FIGURE 4.9: Binary plot of the heterogeneities in the two-dimensional contour plot of Raman Intensity for P3 in PVAc film (a) t_w = 0 and (b) at t_w = 95 min. The black borders were detected by the boxcount algorithm to calculate the fractal dimensions. (c) variation of local fractal dimension d_F as a function of box size (r) (d) the number of boxes (n(r)) versus r, box size and their power law fitting ($n(r) = r^{-d_F}$; dashed red line) which determines the fractal dimension of the polymer.

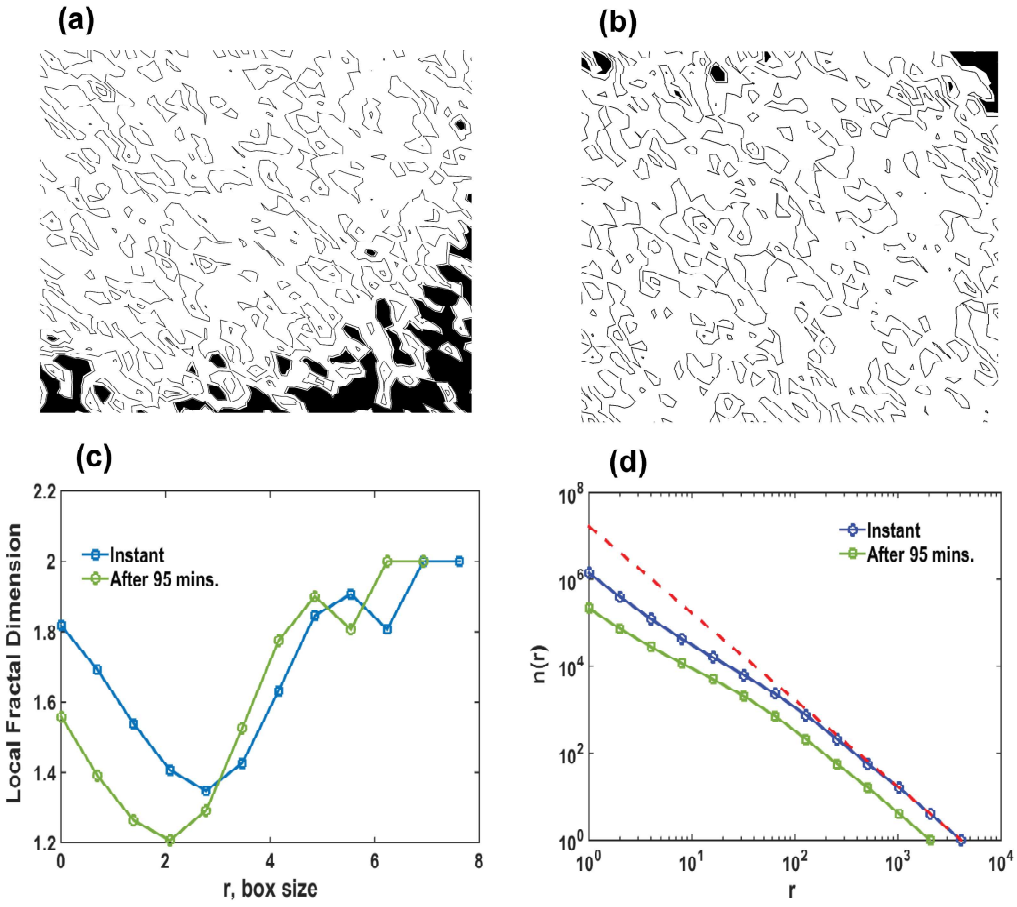

FIGURE 4.10: Binary plot of the heterogeneities in the two-dimensional contour plot of Raman Intensity for P4 representing C-H stretching vibration in PVAc film (a) t_w = 0 and (b) t_w = 95 min. The black borders were detected by the boxcount algorithm to calculate the fractal dimensions. (c) Variation of local fractal dimension d_F as a function of box size (r) (d) the number of boxes (n(r)) versus r, box size and their power law fitting ($n(r) = r^{-d_F}$; dashed red line) which determines the fractal dimension of the polymer.

fractal dimension of boundaries of the clusters was determined using the box-counting algorithm. Then the fractal dimension was calculated using the scaling relation n(r) = r^{d_F} where n(r) was the number of boxes and r was the box size. Figure 4.8 (a) and (b) represents the fractal boundaries for peak 2 in PVAc film at t_w = 0 and t_w = 95 min. The local fractal dimension of these boundaries shows variation with box size as shown in Figure 4.8 (c) and the n(r) versus r plot (Figure 4.8 (d)) helps to determine the fractal dimension (d_F) by a power law fitting of the curve. Similarly, for peak 3 in PVAc film, the boundaries of the cluster domains are determined which is shown in Figure 4.9 (a) and (b) respectively for t_w = 0 and at after t_w = 95 min. The local fractal dimension for peak 3 is given in Figure 4.9 (c) and the power law scaling for d_F is shown in Figure 4.9 (d) for both at t_w = 0 and at t_w = 95 min. Peaks 2 and 3 show similar change in d_F at t_w = 0 and t_w = 95 min. which is given in Table 4.1. This can be due to the fact that they are deconvoluted from a single Raman band which constitutes contribution from various Raman modes present in the main chain as well as the side branch of the polymer. Peak 4, on the other hand represents the C-H stretching vibrational mode, the fractal boundaries for peak 4 are shown in Figure 4.10 (a) and (b) respectively at $t_w = 0$ and t_w = 95 min. From the variation of local fractal dimension (Figure 4.10(c)) and n(r) (Figure 4.10(d)) it is observed that there is higher change in the cluster distribution for at t_w = 0 and at t_w = 95 min. as compared to peak 2 and 3 which can be seen in Table 4.1. Within the errorbars the change in d_F of the clusters is negligible, supporting the simulation results which show that the fractal dimensions in polymer glasses are insensitive of aging during mobile clusters [26]. However, the d_F for all three peaks (peaks 2, 3, and 4) shows a resemblance to d_F = 1.56, the fractal dimension of percolating clusters below the percolation threshold observed for polymers with screened excluded volume interactions having extended configuration [26, 27].

4.5 Spatial and temporal correlations

Apart from the fractal nature of the dynamic heterogeneities, it is evident that there is the presence of CRRs in polymer glass which grows with time after quench and these growing CRRs are associated with the mobility at the molecular level of the polymer. These results are in agreement with the RFOT which predicts the presence of mosaics of CRRs in the glassy state. The glass

TABLE 4.1: Fractal dimension (d_F) for the peaks in PVAc film instantly after quenching (t_w = 0) and after 95 minutes of quenching (t_w = 95 min).

Peak no.	d_F (Instant (t_w = 0))	d_F (after 95 min. (t_w = 95 min))
P2	1.5678 ± 0.19171	1.4767 ± 0.28549
P3	1.5115 ± 0.23592	1.5579 ± 0.27851
P4	1.5999 ± 0.24636	1.5449 ± 0.30661

transition theory as given by RFOT also talks about the presence of spatiotemporal correlations in the CRRs and predicts the evolution of cooperative length scale and timescale on going deeper into the glassy state. The presence of spatiotemporal correlations in the glassy dynamics has been evident in colloidal glasses and several theoretical lennard jones mixtures [7, 18, 28]. Heterogeneous dynamics and correlated motion have also been observed experimentally in polymer glasses [20, 29]. These correlations are therefore important to study and analyze in our system.

Here we have calculated the spatial and temporal fluctuations in the glassy polymer film after quenching it through the glass transition temperature. The temporal correlations as a function of waiting time after quench (t_w) are given in Figure 4.11 for all three peaks appearing in the Raman spectrum of PVAc film. The maximum change in the correlation coefficient ($C(t_w, t+t_w)$) is found in peak 4 which represents the C-H stretching vibrational mode. The $C(t_w, t+t_w)$ is calculated for t_w = 0 secs. to 5696 secs. and t_w = 5700 secs. to 11396 secs. Therefore, two $C(t_w, t+t_w)$ curves are obtained for each peak. It is observed that the two curves are slightly different from each other even though they represent the same peak. This difference in $C(t_w, t+t_w)$ for two different time scales shows that the glassy dynamics is cooperative and it evolves as a function of time after quenching. Similar results were observed from dielectric and polarized fluctuations in PVAc where the correlation function $C(t, t_w)$, followed a stretched exponential behavior as a function of waiting time after quench [19].

2D spatial correlations are also calculated for the three peaks appearing in the Raman spectrum of PVAc film, from the Raman intensity (I_{Max}). The 2D spatial correlation coefficient (C(r,t)) is calculated for two different time scales: at t_w = 0 and at t_w = 95 min. The spatial correlation is calculated along the 340 μm x 340 μm

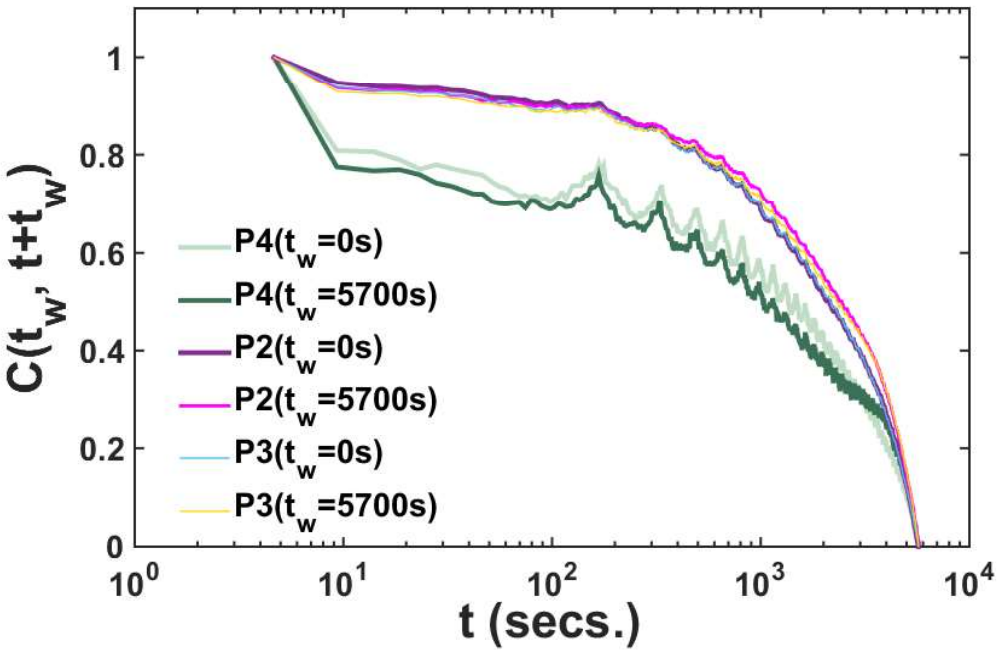

FIGURE 4.11: Intensity correlations as a function of waiting time after a quench for t_w varying between 0 to 5696 secs. and 5700 to 11396 secs. Hence, two $C(t_w, t + t_w)$ curves were obtained for each peak.

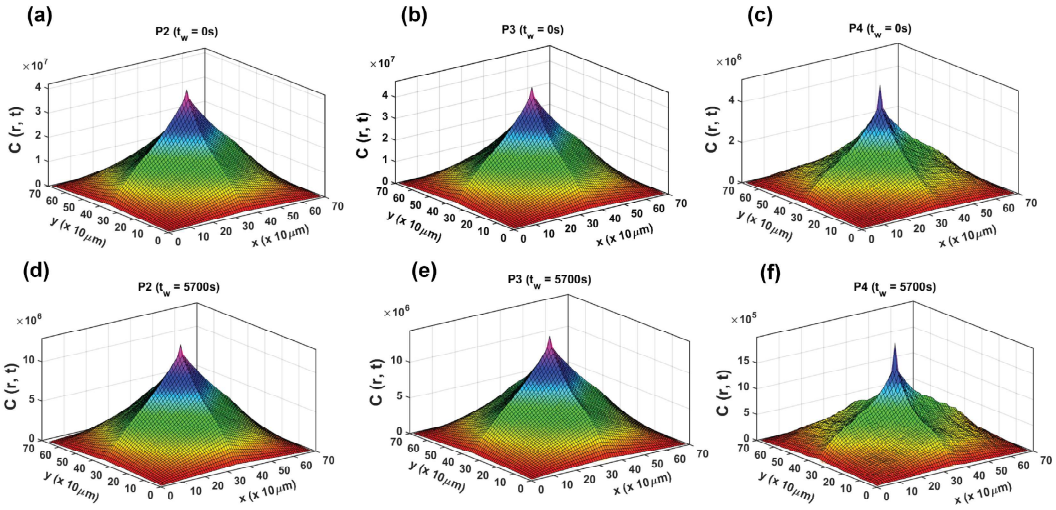

FIGURE 4.12: 2D spatial correlations of I_{Max} in peak 2,3 and 4 instantly after quench (t_w = 0) in (a), (b) and (c) respectively and 95 minutes (5700 secs.) after a quench (t_w = 95 min.) in (d), (e) and (f) respectively.

area on PVAc film. Figure 4.12 (a), (b), and (c) represents the spatial correlations for the peaks 2, 3, and 4 respectively at t_w = 0, and Figure 4.12 (d), (e) and (f) represents the C(r,t) for the peaks 2, 3 and 4 respectively at t_w = 95 min. The sharpness of the peak in the 2D plot describes the higher amount of correlations in the respective peak. Peak 4 representing the C-H vibrational mode shows the highest amount of spatial correlations as compared to the other peaks. This might be due to the contribution of a large number of modes in peaks 2 and 3 which makes it difficult to study a single prominent response from the peaks. It can also be observed that the C(r,t) is higher in the peaks at t_w = 95 min. as compared to the C(r,t) at t_w = 0. This indicates that cooperative relaxation is growing as a function of time after quenching. This behavior is similar to the response in one-dimension temporal correlations as observed in Figure 4.11.

4.6 Experimental dynamic Susceptibility

The dynamic heterogeneities and cooperative nature of glassy dynamics can also be understood from dynamic susceptibility. Here, we have attempted to calculate the experimental dynamic susceptibility from the Raman intensity. Since Raman scattering is an inelastic scattering of electromagnetic radiation with molecular vibration, each Raman intensity is associated with an induced dipole moment which can be used to calculate the dynamic susceptibility. The intensity peaks observed during Raman scattering have a line shape governed by the correlation function of the induced dipole moment, and is the Fourier transform of this correlation function in frequency space, as represented by Equation 4.1. In Stokes scattering, this induced dipole moment has a frequency dependence corresponding to lower frequencies compared to the incident electromagnetic wave.

$$I(\nu) = \frac{1}{2\pi} \int_{-\infty}^{\infty} \frac{< \delta p(t) \delta p(0) > e^{-2\pi i \nu t}}{< p * p > dt} \tag{4.1}$$

Here p(t) is the stochastic-induced dipole moment due to interaction with the incident electromagnetic waves, and p* is its complex conjugate. In practice, the induced dipole moment fluctuates about an average value, and the spontaneous fluctuations are represented by a time-dependent variable, $\delta p(t) = p(t) - < p >$. Then Equation 4.1 can be re-written as follows:

$$I(\nu) = \frac{1}{2\pi} \int_{-\infty}^{\infty} \frac{< \delta p(t) \delta p(0) > e^{-2\pi i \nu t}}{< p^2 > dt} \tag{4.2}$$

The electric field of the incident electromagnetic wave acts as a perturbation, and a response to this perturbation is the dielectric constant, χ(t), which is the ensemble-averaged correlation of the spontaneous fluctuations of the induced dipole moment, $\delta p(t) = p(t) - < p >$, given by the following equation:

$$\chi(t) = \frac{\partial < \delta p(t) \delta p(0) >}{\partial E(t)} = \frac{\partial C(t)}{\partial E(t)} \tag{4.3}$$

In frequency space, the above equation can be written as $\chi(\nu) = \frac{\partial \widetilde{C(\nu)}}{\partial E(\nu)}$, where $\widetilde{C(\nu)}$ is the Fourier transform of the correlation of the spontaneous induced dipole moment fluctuations. From the fluctuation dissipation theorem, which relates the correlations of an observable to the response in the presence of an external perturbation, one can obtain the imaginary part of the response the presence of an external perturbation, one can obtain the imaginary part of the response, which we refer to as dynamic susceptibility, as given by:

$$\chi''(\nu) = \frac{1}{(\nu_L - \nu)^3} (1 - e^{-\frac{hc\nu}{k_B T}}) I(\nu) \tag{4.4}$$

In the above equation, ν_L is the frequency of the incident light in cm^{-1}, so $\nu_L = f_L/c$, where f_L is the frequency of the incident light in Hz, and c is the speed of light. The Stokes Raman shift is obtained as a function of the frequency ν, also in cm^{-1}, h is the Planck's constant, T is the temperature in absolute scale, and k_B is the Boltzmann constant. Dynamic susceptibility $\chi''(\nu)$ is therefore an experimentally measurable quantity, which can be directly obtained from the normalized Stokes intensity as a function of ν.

By using the thermodynamic formulation given in [15] we can write the four-point susceptibility as:

$$\chi_4(T) = \chi''(\upsilon, T)^2 k T^2 / C_p \tag{4.5}$$

In the above equation, C_p (298 K) for polyvinyl acetate = 101.2 Joules/Mole-K and it can be calculated for different temperatures as:

$$C_p^s(T) = C_p^s(T = 298K)[1 + 3x10^{-3}.(T - 298K)] \tag{4.6}$$

The experimental dynamic susceptibility is obtained from the C-H stretching peak (peak 4) appearing in the Raman spectrum of PVAc film because it is the peak that involves contribution from a single vibrational mode which avoids overlapping of the dipole moments of different vibrational modes. The dynamic susceptibility is calculated for both thermal perturbations applied to the polymer film, i.e., thermal ramp and thermal quench.

During thermal ramp, the imaginary part of the experimental dynamic susceptibility, ($\chi^{''}(\nu, T)$) is shown in Figure 4.13 (a). The $\chi^{''}(\nu, T)$ is determined for all the temperatures during the thermal ramp. From the $\chi^{''}(\nu, T)$ versus the Raman frequency (ν) shows an evolution with an increase in the $\chi^{''}(\nu, T)$ spectral intensity at higher temperatures which can also be seen clearly from Figure 4.13 (b) where $\chi^{''}(\nu, T)$ grows as a function of temperature. The temperature dependence of $\chi^{''}(\nu, T)$ also shows a peak after which it starts fluctuating. The four point susceptibility $\chi^4(\nu, T)$ is also calculated from the $\chi^{''}(\nu, T)$, the evolution of $\chi^4(\nu, T)$ as a function of $1/\nu$ is shown in Figure 4.13 (c). Similar to $\chi^{''}(\nu, T)$, $\chi_4(\nu, T)$ spectrum also shows an evolution with increasing temperature during the thermal ramp applied. The growth of $\chi_4(\nu, T)$ as shown in Figure 4.13 (d) is similar to the growth of $\chi^{''}(\nu, T)$ with a maximum and then starts fluctuating. The maxima in $\chi_4(\nu, T)$ is observed around 308 K denoted by $\chi_4^*(T_g)$, which is close to the T_g of PVAc film. This maxima $\chi_4^*(T_g)$ in the $\chi_4(\nu, T)$ curve directly expresses the correlation volume which can be expressed in molecular units [15]. Our results can be compared to the dielectric susceptibility curves and NMR results obtained for other molecular glasses where the susceptibility curve shows a peak showing the presence of the dynamic correlation lengths [21]. The peak of dieletric susceptibility $\chi_4(T)$ also signifies the correlation length in the system. Dielectric spectroscopy experiments on PVAc glass have predicted the correlation length in terms of the number of correlating molecules in the CRRs from the $\chi_4(T)$ [20]. Several other experiments and simulations on colloidal glasses and molecular glasses have also obtained the correlation length from the peak of dielectric susceptibility curve [7, 15, 22].

The variation in experimental dynamic susceptibility is also observed as a function of waiting time after quenching through the glass transition temperature at two different quench rates: 60 °C/min and 100 °C/min. The variation of $\chi^{''}(\nu, T)$ as a function of ν and $\chi_4(\nu, T)$ as a function of $1/\nu$ for the

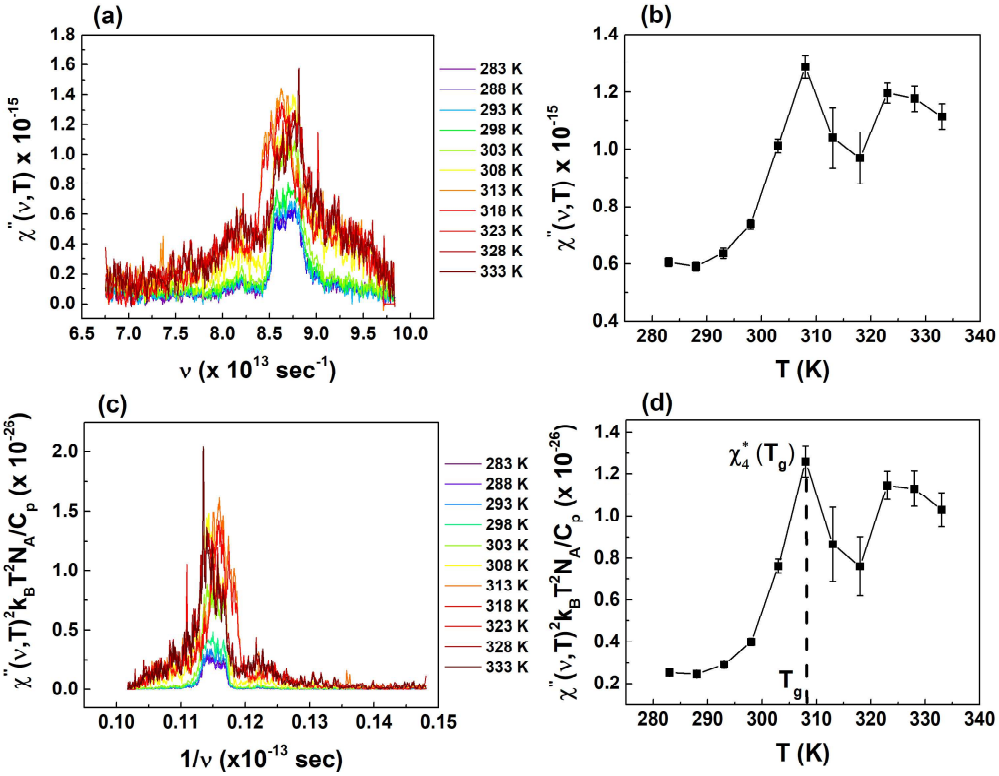

FIGURE 4.13: (a) Evolution of the imaginary part of the experimental dynamic susceptibility $\chi''(\nu, T)$ at different temperatures as a function of the Raman shift ν on subjecting the PVAc film to a slow temperature ramp of rate 10 °C/min. (b) $\chi''(\nu, T)$ grows as a function of T on approaching the glass transition temperature from 333 K, with a maximum at around 308 K. (c) $\chi_4(\nu, T)$ (Equation 8) as a function of $1/\nu$ for different temperatures. (d) $\chi_4(\nu, T)$ shows a peak denoted by $\chi_4^*(T_g)$ around 308 K which is close to the glass transition temperature (T_g).

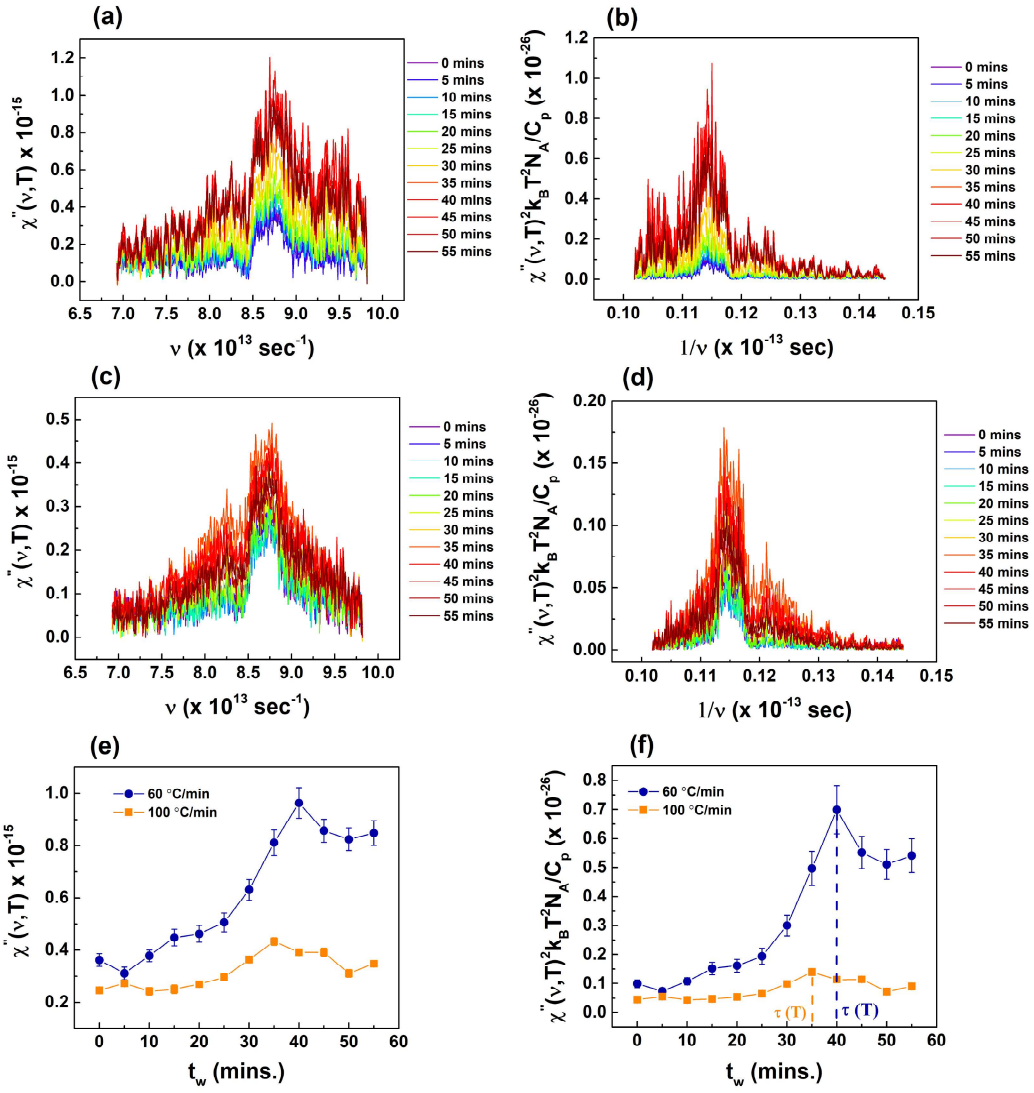

FIGURE 4.14: (a) Evolution of the imaginary part of the experimental dynamic susceptibility $\chi^{''}(\nu, T)$ at the different waiting time (t_w) as a function of the Raman shift ν on subjecting the PVAc film to a temperature quench of rate 60 °C/min. (b) $\chi^4(\nu, T)$ (Equation 8) as a function of $1/\nu$ for different t_w. (c) Evolution of $\chi^{''}(\nu, T)$ for a quench rate 100 °C/min and (d) its $\chi_4(\nu, T)$ as a function of $1/\nu$. (e) and (f) $\chi_4(\nu, T)$ grows as a function of t_w after the quench with maximum denoted by τ(T).

quench rate 60 °C/min is shown in Figure 4.14 (a) and (b) respectively and for the quench rate 100 °C/min is shown in Figure 4.14 (c) and (d) respectively at different time intervals after the quench. It can be observed that the spectrum of both $\chi^{''}(\nu, T)$ and $\chi_4(\nu, T)$ shows an evolution with increasing waiting time (t_w). The t_w dependence of $\chi^{''}(\nu, T)$ and $\chi_4(\nu, T)$ show a continuous increase up to a certain time after which it starts decreasing as shown in Figure 4.14 (e) and (f). The $\chi_4(\nu, T)$ (Figure 4.14(f)) shows a maxima at a certain time denoted by τ(T) which is 40 mins. for the quench rate 60 °C/min and 35 mins. for the quench rate 100 °C/min. The τ(T) for both the quench rates are representative of the time scale where the dynamics is highly correlated. The evolution of dynamic susceptibility for hard and soft colloids has shown similar results where the maxima in $\chi_4(T)$ demonstrates the point where the motion was highly correlated [13]. Therefore, by comparing the $\chi_4(T)$ values with the molecular size of volume fractions one can determine the exact cooperative length scale [13, 15].

4.7 Summary

Raman spectroscopy has become a powerful tool for understanding the glassy dynamics in polymers. The correlations between the Raman modes present in the main chain as well as the side branch of unprocessed polymer and polymer film have established that the molecular motion is cooperative after thermal perturbations. This lays the ground for the presence of dynamic heterogeneities in the glassy state of the polymer. The 2-D map of the polymer film using Raman scattering reveals the presence of heterogeneous domains with variable intensity where the domains with less and high contribution from the respective molecular modes were directly observed. These heterogeneous domains evolve after quenching through the glass transition temperature, evident from the time-resolved 2-D contour map of the polymer film at t_w = 0 and t_w = 95 min. The growth of the heterogeneous domains after thermal quench is evidence of the presence of dynamic heterogeneities in the glassy state of a polymer film. Such growth of medium-range crystalline order has previously been observed using molecular dynamics simulations of supercooled liquids [30]. The dynamic heterogeneities in the polymer film after thermal perturbation also show cooperativity between the dynamically relaxing domains. The presence of

spatial and temporal correlations is a signature of the cooperative behavior of the relaxing heterogeneous domains. The peak in the growth of dynamic susceptibility as a function of temperature and time give an idea of the correlation length in the system. The results provide direct evidence of the presence of dynamic heterogeneities at the molecular scale of a polymer glass and they also suggest that Raman spectroscopy is an effective tool to experimentally investigate the glassy dynamics.

Refernces

[1] Ludovic Berthier and Giulio Biroli. Theoretical perspective on the glass transition and amorphous materials. *Reviews of modern physics*, 83(2):587, 2011.

[2] Mark D Ediger, C Austen Angell, and Sidney R Nagel. Supercooled liquids and glasses. *The journal of physical chemistry*, 100(31):13200–13212, 1996.

[3] C Austin Angell, Kia L Ngai, Greg B McKenna, Paul F McMillan, and Steve W Martin. Relaxation in glassforming liquids and amorphous solids. *Journal of applied physics*, 88(6):3113–3157, 2000.

[4] Gerold Adam and Julian H Gibbs. On the temperature dependence of cooperative relaxation properties in glass-forming liquids. *The journal of chemical physics*, 43(1):139–146, 1965.

[5] TR Kirkpatrick and D Thirumalai. Colloquium: Random first order transition theory concepts in biology and physics. *Reviews of Modern Physics*, 87(1):183, 2015.

[6] Indrajit Tah, Anoop Mutneja, and Smarajit Karmakar. Understanding slow and heterogeneous dynamics in model supercooled glass-forming liquids. *ACS omega*, 6(11):7229–7239, 2021.

[7] K Hima Nagamanasa, Shreyas Gokhale, AK Sood, and Rajesh Ganapathy. Direct measurements of growing amorphous order and non-monotonic dynamic correlations in a colloidal glass-former. *Nature Physics*, 11(5):403–408, 2015.

[8] Agnes Duri and Luca Cipelletti. Length scale dependence of dynamical heterogeneity in a colloidal fractal gel. *EPL (Europhysics Letters)*, 76(5):972, 2006.

[9] GBJP Biroli, J-P Bouchaud, Andrea Cavagna, Tomás S Grigera, and Paolo Verrocchio. Thermodynamic signature of growing amorphous order in glass-forming liquids. *Nature Physics*, 4(10):771–775, 2008.

[10] Hailin Yuan, Jinsong Yan, Ping Gao, Sanat K Kumar, and Ophelia KC Tsui. Microscale mobile surface double layer in a glassy polymer. *Science Advances*, 8(45):eabq5295, 2022.

[11] L Cipelletti and ER Weeks. Dynamical heterogeneities in glasses, colloids and granular media, 2011.

[12] Antonio Coniglio, Tiziana Abete, Antonio De Candia, Emanuela Del Gado, and Annalisa Fierro. Dynamical heterogeneities: from glasses to gels. *Journal of Physics: Condensed Matter*, 20(49):494239, 2008.

[13] Y Rahmani, K Van Der Vaart, B Van Dam, Z Hu, V Chikkadi, and P Schall. Dynamic heterogeneity in hard and soft sphere colloidal glasses. *Soft Matter*, 8(15):4264–4270, 2012.

[14] Dapeng Bi, JH Lopez, Jennifer M Schwarz, and M Lisa Manning. A density-independent rigidity transition in biological tissues. *Nature Physics*, 11(12):1074–1079, 2015.

[15] L. Berthier, G. Biroli, J.-P. Bouchaud, L. Cipelletti, D. El Masri, D. L'Hôte, F. Ladieu, and M. Pierno. Direct experimental evidence of a growing length scale accompanying the glass transition. *Science*, 310(5755):1797–1800, 2005.

[16] Kenji Yoshimoto, Tushar S Jain, Kevin Van Workum, Paul F Nealey, and Juan J de Pablo. Mechanical heterogeneities in model polymer glasses at small length scales. *Physical review letters*, 93(17):175501, 2004.

[17] Claudia Artiaco, Federico Balducci, Markus Heyl, Angelo Russomanno, and Antonello Scardicchio. Spatiotemporal heterogeneity of entanglement in many-body localized systems. *Physical Review B*, 105(18):184202, 2022.

[18] Mohit Sharma, Manoj Kumar Nandi, and Sarika Maitra Bhattacharyya. Identifying structural signature of dynamical heterogeneity via the local softness parameter. *Physical Review E*, 105(4):044604, 2022.

[19] Hassan Oukris and NE Israeloff. Nanoscale non-equilibrium dynamics and the fluctuation–dissipation relation in an ageing polymer glass. *Nature Physics*, 6(2):135–138, 2010.

[20] Bidur Rijal, Laurent Delbreilh, and Allisson Saiter. Dynamic heterogeneity and cooperative length scale at dynamic glass transition in glass forming liquids. *Macromolecules*, 48(22):8219–8231, 2015.

[21] N Petzold, B Schmidtke, R Kahlau, D Bock, R Meier, B Micko, Danuta Kruk, and EA Rössler. Evolution of the dynamic susceptibility in molecular glass formers: Results from light scattering, dielectric spectroscopy, and nmr. *The Journal of chemical physics*, 138(12):12A510, 2013.

[22] Hua Tong and Hajime Tanaka. Revealing hidden structural order controlling both fast and slow glassy dynamics in supercooled liquids. *Physical Review X*, 8(1):011041, 2018.

[23] Durval Bertoldo Menezes, Andreas Reyer, Alexandre Marletta, and Maurizio Musso. Determination of the temperatures of the γ, β and α relaxation processes in nylon 6, 6 by raman spectroscopy. *Polymer*, 106:85–90, 2016.

[24] J Yi and J Jonas. Raman study of vibrational and rotational relaxation of liquid benzene-d 6 confined to nanoporous silica glasses. *The Journal of Physical Chemistry*, 100(42):16789–16793, 1996.

[25] Yoshiharu Suzuki and Yasunori Tominaga. Polarized raman spectroscopic study of relaxed high density amorphous ices under pressure. *The Journal of chemical physics*, 133(16):164508, 2010.

[26] TA Vilgis. Flory theory of polymeric fractals-intersection, saturation and condensation. *Physica A: Statistical Mechanics and its Applications*, 153(3):341–354, 1988.

[27] D Stauffer and A Aharony. Introduction to percolation theory; e-book, 2018.

[28] Smarajit Karmakar, Chandan Dasgupta, and Srikanth Sastry. Analysis of dynamic heterogeneity in a glass former from the spatial correlations of mobility. *Phys. Rev. Lett.*, 105:015701, Jul 2010.

[29] Heiko Conrad, Felix Lehmkuehler, Birgit Fischer, Fabian Westermeier, MA Schroer, Yuriy Chushkin, Christian Gutt, Michael Sprung, and Gerhard Gruebel. Correlated heterogeneous dynamics in glass-forming polymers. *Physical Review E*, 91(4):042309, 2015.

[30] Indrajit Tah, Shiladitya Sengupta, Srikanth Sastry, Chandan Dasgupta, and Smarajit Karmakar. Glass transition in supercooled liquids with medium-range crystalline order. *Physical review letters*, 121(8):085703, 2018.